ACS OMEGA

Open Access

http://pubs.acs.org/journal/acsodf

Article

Exploring the Impact of Al_2O_3 Additives in Gasoline on HCCI-DI Engine Performance: An Experimental, Neural Network, and Regression Analysis Approach

Lionus Leo George Mary, Subramanian Manivel,* Shalini Garg, Vinoth Babu Nagam, Komal Garse, Ranjit Mali, T. M. Yunus Khan, and Rahmath Ulla Baig

Cite This: *ACS Omega* 2023, 8, 47701−47713

Read Online

ACCESS | Metrics & More | Article Recommendations

ABSTRACT: This study delves into the influence of incorporating alumina (Al_2O_3) nanoparticles with waste cooking oil (WCO) biofuels in a gasoline engine that employs premixed fuel. During the suction phase, gasoline blends with atmospheric air homogeneously at the location of the inlet manifold. The biodiesel, enhanced with Al_2O_3 nanoparticles and derived from WCO, is subsequently directly infused into the combustion chamber at 23° before the top dead center. The results highlight that when gasoline operates in the homogeneous charge compression ignition with direct injection (HCCI-DI) mode, there is a notable enhancement in thermal efficiency by 4.23% in comparison to standard diesel combustion. Incorporating the Al_2O_3 nanoparticles with the WCO biodiesel contributes to an extra rise of 6.76% in thermal efficiency. Additionally, HCCI-DI combustion paves the way for a reduction in nitrogen oxides and smoke emissions, whereas biodiesel laced with Al_2O_3 nanoparticles notably reduces hydrocarbon and carbon monoxide discharges. Predictive tools such as artificial neural networks and regression modeling were employed to forecast engine performance variables.

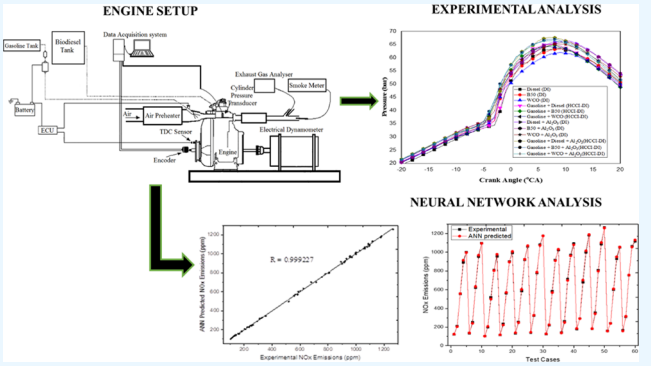

1. INTRODUCTION

HCCI combustion technology offers a potential strategy for lowering emissions and enhancing the thermal efficiency of IC engines. It is favored for its ability to decrease NOx emissions and boost thermal efficiency due to its homogeneous fuel−air mixture and igniting by the compression process. When suction stroke occurs, gasoline and air are combined in the air intake manifold of the engine and then supplied to the engine. The mixture is compressed and abruptly ignites during compression stroke, initiating the combustion process. Heat is rapidly released when all of the air and gasoline in the chamber of combustion burn at the same time, resulting in combustion that is closer to a constant volume combustion. Finally, HCCI technology has the potential to cut emissions while also enhancing internal combustion engine performance and saving precious fuel supplies.[1]

Onishi et al. first proposed the idea of combustion of the HCCI called ATAC in 1979 and demonstrated its capability to deliver stable combustion with lean fuel mixtures during a partial throttle operation. They also highlighted improvements in fuel efficiency and reduction in emissions in two-stroke cycle SI engines, resulting in decreased noise and vibration.[2] Noguchi et al. put forward the HCCI concept as Toyota−Soken (TS) burning occurs in a petrol engine with two strokes, demonstrating its stability and low hydrocarbon emissions, as well as decreased consumption of fuel.[3] Najt and Foster discovered that kinetics of chemicals is crucial in a four-stroke engine, particularly during combustion of HCCI.[4] Norimasa Iida investigated the combustion mechanism of ATAC in a two-stroke SI engine and observed uniform ignition in the combustion chamber.[5] According to research by Magnus Christensen et al., any form of liquid fuel may be utilized in an adjustable ratio of compression HCCI engine using a pair of fuel port injection systems.[6]

Although HCCI combustion technology has demonstrated its effectiveness in lowering NOx emissions and improving thermal efficiency, researchers have encountered various challenges when operating HCCI engines under high loads and speeds, features like increased banging, greater HC and CO emissions, and issues with the air and gasoline mixture's

Received: August 12, 2023
Revised: November 21, 2023
Accepted: November 23, 2023
Published: December 7, 2023

Table 1. Fuel Properties

fuel blend	density (kg/m^3), at 15 °C	kinematic viscosity (mm^2/s), at 40 °C	flash point (°C)	fire point (°C)	calorific value (kJ/kg)
gasoline	750	0.494	−43	62	45,120
diesel	840	3.122	61.5	73	42,980
B50	861	3.167	78.3	82	38,655
WCO	875	4.214	182	194	36,540
diesel + Al_2O_3	839	3.081	58.5	72	43,890
B50 + Al_2O_3	860	3.161	74.2	81	39,128
WCO + Al_2O_3	874	4.178	175	190	37,455
standard test method	ASTM D1298	ASTM D445	ASTM D93	ASTM D93	ASTM D240

nonhomogeneity in the intake manifold.[7] In a quest to address these quandaries, scholars have delved into an array of techniques, such as implementing exhaust gas recirculation (EGR), wielding turbocharging/supercharging, increasing the fuel's injection pressure, fine-tuning the compression rate, and augmenting suction air to magnify the power of HCCI engines.[8−20]

HCCI combustion technology has captured researchers' attention as a promising way to reduce emissions and augment thermal efficiency in IC engines. However, one of the crucial limitations of HCCI technology is the absence of a trigger, beginning of burning (SOC), which sometimes restricts its use to specific speed and load conditions. To overcome this challenge, researchers have developed, with a homogeneous premixed charge, the HCCI-DI ignition mode that combines the benefits of HCCI and DI combustion, similar to HCCI, and direct fuel injection, like in DI. According to studies, in terms of operational range, peak pressure in the cylinder, as well as the highest heat discharge rate, the HCCI-DI burning mode performs better than the standard HCCI burning mode. Researchers have also explored methods like recirculating exhaust gas, second fuel injection timing, premixed equivalency ratio, and other parameters to enhance the performance of HCCI-DI combustion.[21−23]

Utilizing methyl ester made from discarded frying oil as a renewable fuel in CI engines has drawn interest because of its sustainability and capacity for addressing waste disposal problems through recycling. Research has examined the outcomes of using WCO effects of biodiesel on the process of combustion, pollutants, and engine efficiency. Results show that the engine's thermal efficiency remains unchanged despite improved emission characteristics.[24,25] Although WCO biodiesel-powered engines show a decrease in carbon monoxide (CO) and hydrocarbons (HCs), they also exhibit an increase in nitrogen oxide (NOx) emissions.[26]

Many research studies have looked into the impact of adding nanosized substances, such as alumina, cerium, carbon nanotubes, manganese, and magnesium, to engines and have found that these additives can result in enhanced engine efficiency and lowered emissions.[27−33] This research used an Al_2O_3 fuel additive based on alumina to boost the engine's overall performance.

The use of artificial neural networks (ANNs) has gained widespread popularity as a method for modeling IC engines due to advancements in computer technology. These models deliver accurate results while minimizing the computational time and resources needed. Numerous researchers have created ANN models to estimate engine efficiency and exhaust emission characteristics, and observations have shown that the inaccuracies in the predictions are acceptable.[34−43] Artificial neural networks (ANNs) have become a widely accepted tool for modeling internal combustion engines (IC engines) due to advancements in computer technology. ANN models yield precise results while minimizing the amount of computational exertion and resources. Various scholars have developed ANN models to predict emissions from the exhaust and engine efficiency aspects, and their findings indicate that the discrepancies in prognoses lie within tolerable thresholds.

The novelty of this research lies in the unique combination of waste cooking oil (WCO) biodiesel and Al_2O_3 nanoparticles in an HCCI-DI engine setup, which has not been previously explored to date. Additionally, the innovative use of a blended gasoline charge of 20% with this fuel mixture offers a distinctive approach toward addressing combustion challenges in HCCI engines. Furthermore, the incorporation of both regression modeling and artificial neural network (ANN) techniques to predict engine outputs showcases a comprehensive methodological approach to deciphering complex combustion phenomena. This investigation presents a novel outlook on enhancing the performance and emission characteristics of HCCI-DI engines, potentially paving the way for more sustainable and efficient combustion engines in the future.

2. FUEL PREPARATION

One of the problems encountered when using WCO as fuel for engines is its viscosity, which is due to its heavy molecular weight. This increased viscosity leads to size-reduced vaporization and a narrower spray angle, all of which can have a negative impact on engine performance. To address this issue, researchers have explored treatments aimed at reducing the viscosity of WCO. One used method is transesterification, which involves converting WCO into fatty esters (methyl and ethyl esters) through a reaction with alcohol. In this study, ultrasonic blending was employed to mix the WCO diesel blend and the specifications of the resulting biodiesels are presented in Table 1.

3. EXPERIMENTAL SETUP

In this study, an Al_2O_3 nanoadditive was prepared from micrometer-scale Al_2O_3 powder using a ball-milling machine. The micrometer-scale Al_2O_3 powder was obtained from a supplier specializing in chemical and laboratory products. The desired quantity of Al_2O_3 powder was measured and loaded into the ball-milling machine along with milling media, such as small steel balls. The milling process commenced, subjecting the powder and milling media to high-energy impacts and grinding action. Over 10 h, the micrometer-scale Al_2O_3 particles underwent significant size reduction, forming nanoscale Al_2O_3 particles. The rotational movement of the milling machine facilitated the breakage and refinement of particles, transforming them into the desired nanoadditive. After the milling process, the resulting Al_2O_3 nanoadditive was carefully

https://doi.org/10.1021/acsomega.3c05959
ACS Omega 2023, 8, 47701−47713

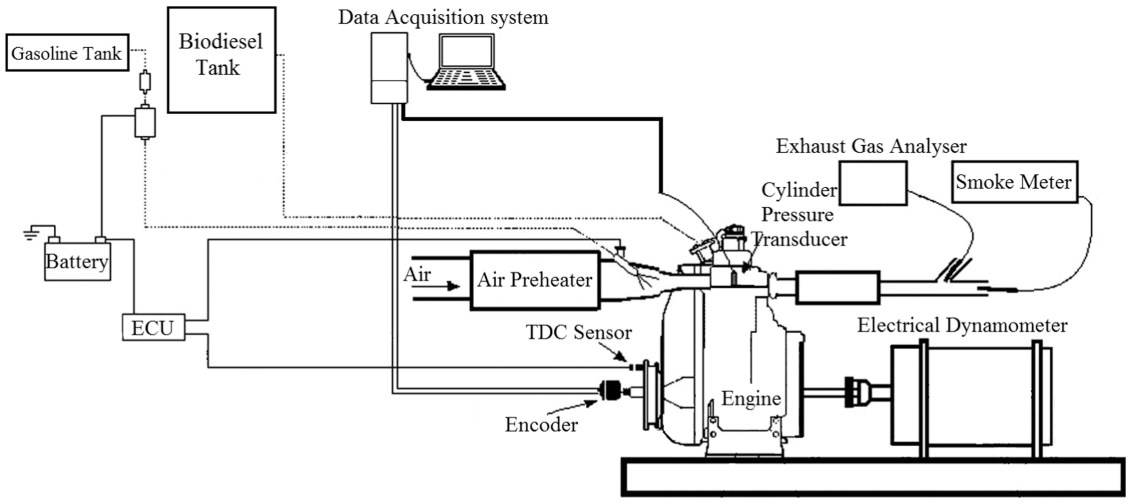

Figure 1. Diagrammatic representation of the experimental setup.

extracted from the milling machine. Additional steps, such as sieving or sonication, were employed to ensure a uniform particle size and to prevent agglomeration.

In this investigation, an unforced solitary-chamber diesel motor was employed to delve into the repercussions of the Al_2O_3 additive in a gasoline-infused WCO-fueled HCCI-DI engine. Figure 1 portrays the arrangement of the engine setup, and Table 2 enumerates the engine particulars. In order to ensure uniform fuel dispersal, a supplementary fuel injection system was implemented. This system encompasses a fuel injector, reservoir, pump, and electronic control unit. The motor's intake manifold was outfitted with a fuel injector, and a distinct fuel reservoir furnished homogeneous petrol for the suction stroke. The electronic control unit managed the timing and volume of the fuel injection. The engine's intake manifold was heated to a constant 60 °C temperature by an electronic air preheater. Engine testing at various loads was performed using a swing field electrical dynamometer.

Table 2. Engine Specifications

parameter	specification
engine type	single-cylinder naturally aspirated engine
rated power	4.4 kW
rated speed	1500 rpm
compression ratio	17.5:1
bore	87.5 mm
stroke	110 mm
injection timing of direct injection fuel	23° before TDC

To evaluate the performance and emissions of the engine, a variety of tools were used. To monitor the input and output temperatures of the engine, thermocouples and an LCD temperature monitor were used. Using an orifice meter, the engine's air intake was measured. A surge tank was installed on the intake channel of the engine to reduce cyclic changes and maintain a consistent airflow through the oximeter. An AVL GH14D/AH01 piezoelectric pressure detector was used to measure the in-cylinder pressure at 0.5 °CA, and a high-speed data collection system was used to record 50 cycles of the cylinder pressure-crank angle for each experimental condition. The engine's crank angle was calculated using an AVL 365C, while NOx, UHC, CO, CO_2, and O_2 emissions were measured using an AVL DI GAS 444 five-gas analyzer, and the smoke capacity was determined using an AVL 415 smoke detector.

4. UNCERTAINTY ANALYSIS

Experiments and performance parameter calculations can involve uncertainty. Environmental circumstances, observations, calibration, equipment, and test orders cause error and uncertainty. Uncertainty analysis proved that measurement instruments were accurate. Table 3 shows instrument uncertainty percentages.

Equation 1 estimates the experiment's uncertainty.[28]

$$\%\delta = [(\delta_{\text{pressure transducer}})^2 + (\delta_{\text{crank angle encoder}})^2 + (\delta_{\text{HC}})^2 + (\delta_{\text{CO}})^2 + (\delta_{\text{CO}})^2 + (\delta_{\text{smoke}})^2 + (\delta_{\text{K-2 thermocouple}})^2 + (\delta_{\text{stop watch}})^2 + (\delta_{\text{manometer}})^2 + (\delta_{\text{burette}})^2]^{1/2} \quad (1)$$

$$\%\delta = (0.01^2 + 0.2^2 + 0.25^2 + 0.2^2 + 0.35^2 + 0.2^2 + 0.35^2 + 1^2 + 0.2^2 + 0.2^2 + 1.5^2 + 1.5^2)^{1/2} = \pm 2.451\%$$

5. EXPERIMENTAL PROCEDURE

Prior to the test, the engine was brought to a certain temperature for the lubricating oil, coolant, and electric air preheater. At loads ranging from 0 to 100% of the engine's total capacity, the research examined the diesel ignition and HCCI-DI combustion modes. 1500 rpm was the constant speed used for all studies. Then, three different fuels with four different combinations were prepared: the first combination was of diesel, B50, and WCO biodiesel; the second combination was of diesel, B50, and WCO biodiesel mixed with gasoline; the third combination was of diesel, B50, and WCO biodiesel mixed with Al_2O_3; and the fourth combination was of diesel, B50, and WCO biodiesel mixed with gasoline and Al_2O_3. These were injected into the diesel engine, and the performance and emission characteristics of different blends were analyzed.

https://doi.org/10.1021/acsomega.3c05959
ACS Omega 2023, 8, 47701−47713

Table 3. Instruments and Their Range, Accuracy, and Uncertainty Percentage

instrument	measuring range	accuracy	% δ
AVL GH14D/AH01 piezoelectric pressure transducer	0−250 bar	±0.01 bar	±0.01
AVL 365C crank angle encoder		±1°	±0.2
AVL DI GAS 444 five-gas analyzer			
NOx	0−5000 ppm vol	<500 ppm vol: ±50 ppm vol	±0.25
		>500 ppm vol: ±10%	
HC	0−20,000 ppm vol	<200 ppm vol: ±10 ppm vol	±0.2
		>200 ppm vol: ±5%	
CO	0−10% vol	<0.6% vol: ±0.03% vol	±0.35
		>0.6% vol: ±5%	
CO_2	0−20% vol	<10% vol: ±0.5% vol	±0.2
		>10% vol: ±5%	
O_2	0−22% vol	<2% vol: ±0.1% vol	±0.35
		>2% vol: ±5%	
AVL 415 smoke meter			
smoke intensity	0−10 FSN	0.002 FSN	±1
K-2 thermocouple	0−1250 °C	±1 °C	±0.2
digital stopwatch		±0.2 s	±0.2
U-tube manometer		±1 mm	±1.5
buret	1−30 cm^3	±0.2 cm^3	±1.5

6. RESULTS AND DISCUSSION

6.1. Characteristics of Combustion. To investigate combustion, in-cylinder pressure readings were made. The raw pressure data were smoothed down to remove any noise that could have been present in the data. The smoothing technique utilized in this study is demonstrated in eq 2.

$$P_n = \frac{(P_{n-1} + 2(P_n) + P_{n+1})}{4} \quad (2)$$

The rate of pressure rise (RPR) was calculated from eq 3

$$\frac{dP}{d\theta} = \frac{(P_{n-2}) - 8(P_{n+1}) - (P_{n+2})}{12(\Delta\theta)} \quad (3)$$

The HRR was calculated by using an initial law analysis. The HRR has been described in eq 4.

$$\text{HRR} = \left(\frac{\gamma}{\gamma - 1} \times P \times \frac{dV}{d\theta}\right) + \left(\frac{1}{\gamma - 1} \times V \times \frac{dP}{d\theta}\right) \quad (4)$$

The combustion process was evaluated using the pressure of the cylinder readings. The pressure data were processed to eliminate noise. Under maximum engine load, Figure 2 illustrates the cylinder variations in pressure during burning of DI and HCCI-DI both before and after the addition of Al_2O_3. As additional fuel burns, the cylinder pressure rises as the engine load rises in the combustion chamber. When utilizing WCO biodiesel, the start of combustion (SOC) increases since it has a higher viscosity and more oxygen. Furthermore, a higher proportion of WCO biodiesel resulted in a lower peak pressure value (P_{max}). For DI combustion, B50, and WCO, the P_{max} values were 63.294, 63.412, and 62.034 bar, respectively. The reduced calorific content of WCO biodiesel may be the cause for the lower P_{max} readings.

The pressure change within the cylinder was examined in the study for combustion scenarios for DI and HCCI-DI with and without the addition of Al_2O_3. The cylinder pressure increased as more petrol burnt in the burning chamber and the engine's load increased. The introduction of WCO biodiesel enhanced the start of combustion (SOC), but because of its reduced calorific value, it led to lower peak pressure values (P_{max}). When compared to DI combustion, the delay duration in HCCI-DI combustion with petrol premixing was shortened by up to 2 °CA, which resulted in greater P_{max} values and an advanced crank angle value matching P_{max}. Due to the

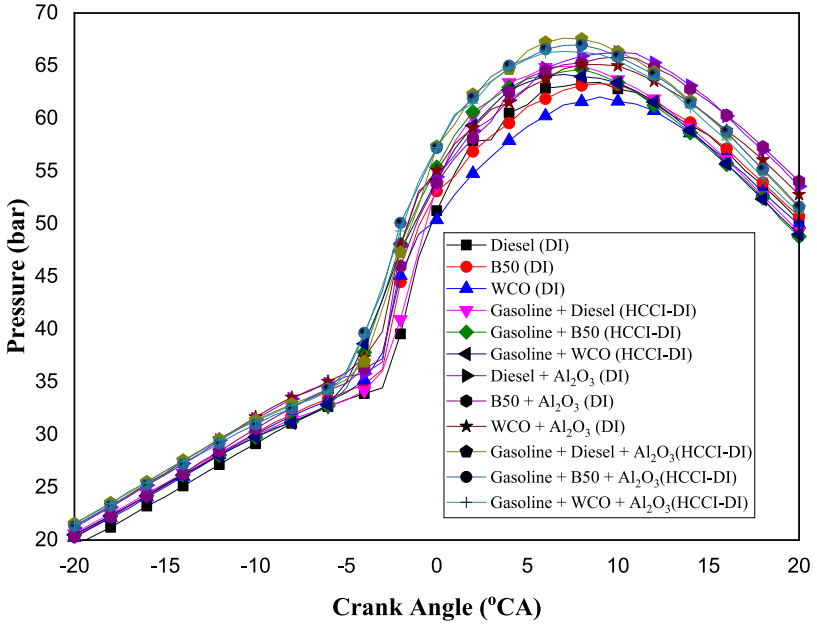

Figure 2. Effects of Al_2O_3 on pressure.

https://doi.org/10.1021/acsomega.3c05959
ACS Omega 2023, 8, 47701−47713

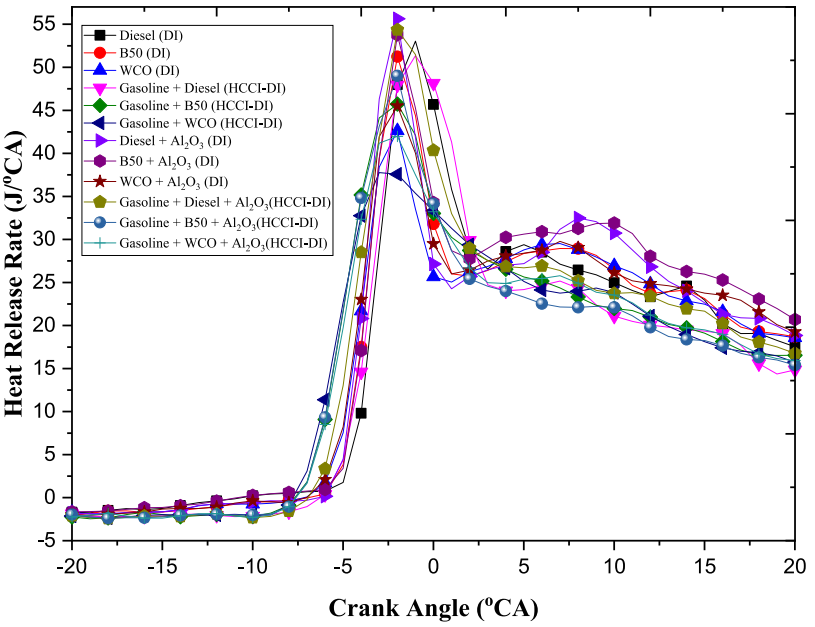

Figure 3. Effects of Al_2O_3 on HRR.

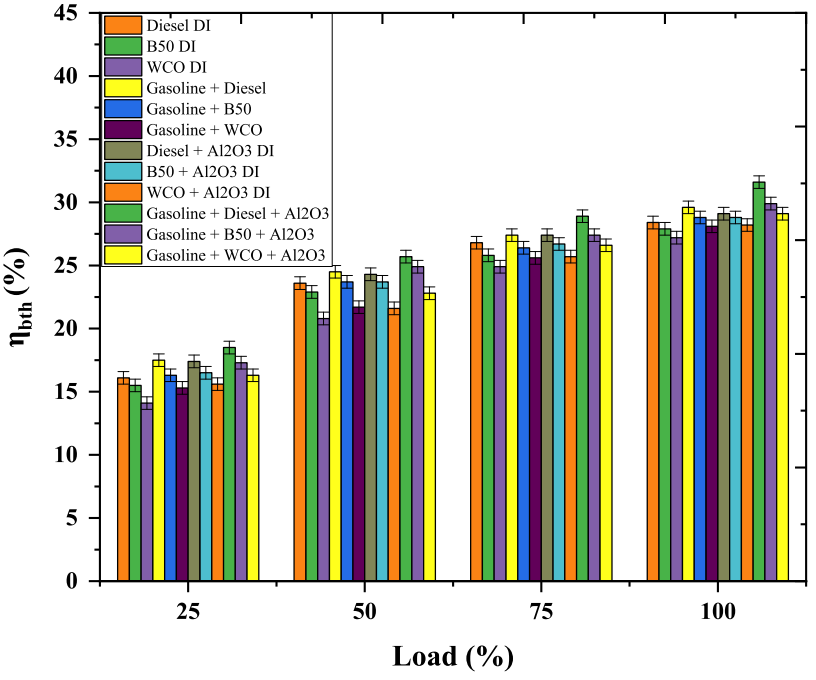

Figure 4. Effects of Al_2O_3 on η_{bth}.

homogeneous mixture and high heat content of the petrol in the combustion chamber, the P_{max} in HCCI-DI combustion increased.

Higher DI combustion peak pressure values (P_{max}) were obtained with Al_2O_3 addition. It was discovered that the diesel, B50, and WCO biodiesel that had been mixed with Al_2O_3 had P_{max} values of 66.264, 65.848, and 65.107 bar, respectively. HCCI-DI combustion with the Al_2O_3 additive showed an improvement in P_{max} and a 2 °CA advance in the crank angle at the peak pressure (P_{max}) as compared to DI combustion. Diesel, B50, and WCO have P_{max} values for HCCI-DI combustion with Al_2O_3 values of 67.623, 66.976, and 66.356 bar, respectively.

The variation in the HRR in Figure 3 depicts the combustion of DI and HCCI-DI both before and after the addition of Al_2O_3. As the WCO biodiesel percentage increased, the HRR_{max} values for both combustion modes fell. In comparison to diesel, which had an HRR_{max} of 53.02 J/°CA at the maximum load, WCO biodiesel had a 42.61 J/°CA at the maximum load. This decrease in HRR_{max} is likely to be caused by WCO biodiesel's quicker ignition and lower calorific value, which may prolong the combustion time and limit heat release. Lower HRR_{max} values were also seen in the HCCI-DI combustion of petrol premixed WCO biodiesel, with corresponding HRR_{max} values of 37.75 J/°CA and 42.61 J/°CA for HCCI-DI and DI combustion. The prolonged

https://doi.org/10.1021/acsomega.3c05959
ACS Omega 2023, 8, 47701−47713

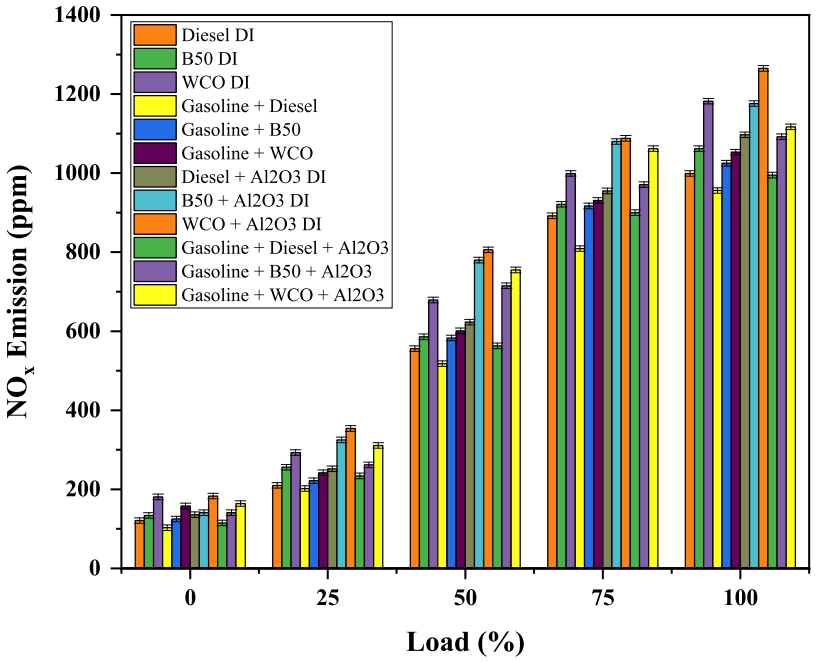

Figure 5. Effects of Al_2O_3 on NOx.

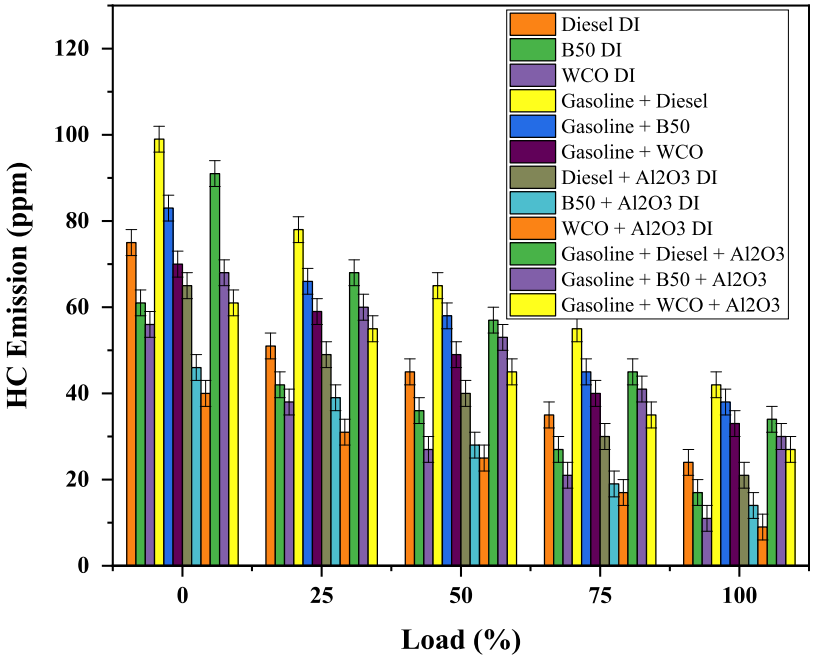

Figure 6. Effects of Al_2O_3 on HC.

burning duration in the HCCI-DI process may account for the decline in HRR_{max}.

The study's findings show that when utilized in direct injection and HCCI-DI combustion instead of diesel fuel, biodiesel made from wasted culinary oil (WCO) produces lower maximum pressure values (P_{max}) and HRR_{max}. However, the addition of an Al_2O_3 additive boosted the P_{max} and HRR_{max} for WCO biodiesel and improved the combustion characteristics. The lower calorific value and earlier start of combustion (SOC) of WCO biodiesel were blamed for the decrease in P_{max} and HRR_{max}. The HCCI-DI combustion method with petrol premixing was found to advance the crank angle value corresponding to P_{max} and create higher P_{max} values when compared to DI combustion. The catalytic effect of the Al_2O_3 additive was seen as a potential explanation for the rise in the P_{max} and HRR_{max} values.

6.2. Performance Characteristics. The experimental findings depicted in Figure 4 demonstrate that when the load increases, the braking thermal efficiency of the DI and HCCI-DI engines rises. The homogeneous, thin, lower-temperature combustion in the 3HCCI-DI process with petrol premixing results in a higher η_{bth}. In addition, it was found that mixing Al_2O_3 with WCO biodiesel improved the η_{bth} of the engine. When compared to the HCCI-DI process without Al_2O_3 addition, the η_{bth} of the diesel fuel increased by up to

https://doi.org/10.1021/acsomega.3c05959
ACS Omega 2023, 8, 47701−47713

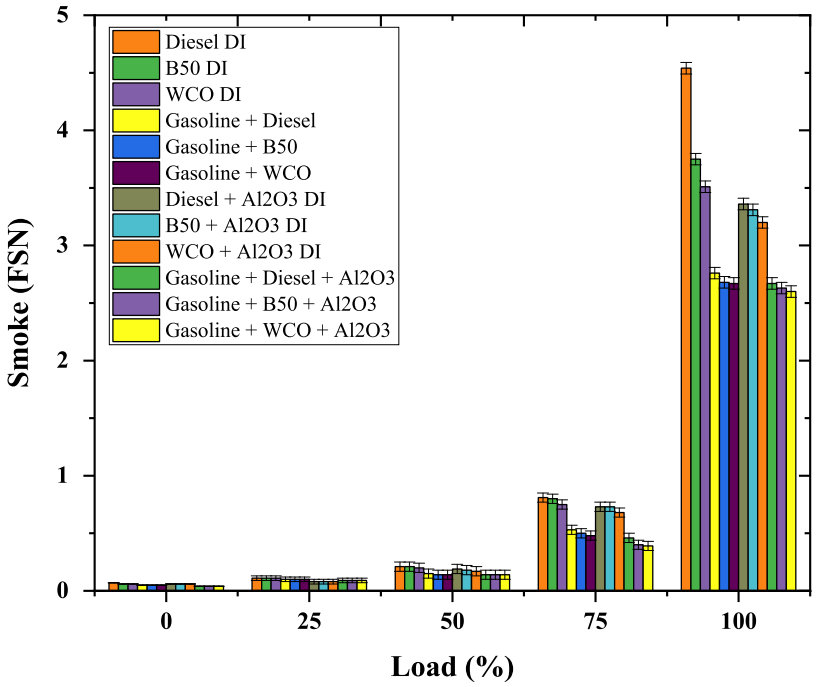

Figure 7. Effects of Al_2O_3 on smoke.

6.76% when Al_2O_3 was added to it. However, the low calorific content of WCO biodiesel results in a small decrease in η_{bth}.

6.3. Emission Characteristics. As engine load increases, it is observed that NOx emissions correspondingly rise. The underlying reason for this relationship can be linked directly to fuel combustion dynamics. With higher loads, engines require a greater amount of fuel. As this fuel is combusted, it results in an elevation of the cylinder temperature. This heightened temperature, combined with the nitrogen present in air, facilitates the formation of nitrogen oxides, commonly referred to as NOx. The combustion processes for direct ignition and HCCI-DI are affected by the Al_2O_3 additive, as shown in Figure 5. In our comprehensive study, a notable trend was observed regarding the usage of waste cooking oil (WCO) biodiesel: as the production of this biodiesel increased, there was a concomitant rise in NOx emissions. Several factors are believed to be at play here. WCO biodiesel inherently possesses a higher viscosity compared to conventional diesel. This characteristic can lead to the creation of localized zones within the combustion chamber, where intense heat is generated. These "hotspots" promote fuel-rich combustion zones, which are prime areas for elevated NOx generation. Further compounding this effect is the enhanced oxygen content found in the WCO biodiesel. A richer oxygen environment generally augments the combustion efficiency and process. However, while this can offer advantages in terms of energy extraction from the fuel, it also contributes to the rise in NOx emissions due to the increased availability of oxygen, aiding the formation of nitrogen oxides during combustion. However, not all findings were leaning toward higher emissions. When we transitioned to the homogeneous charge compression ignition-direct injection (HCCI-DI) engine, which incorporates a mechanism for fuel premixing, we witnessed a promising reduction in the number of NOx emissions. This engine, with its hallmark lean and low-temperature combustion dynamics, can significantly diminish the production of NOx. Specifically, our experiments showcased that NOx emissions from the HCCI-DI engine, when powered with WCO, plummeted by 10.91% when juxtaposed against traditional DI combustion. However, the scenario altered when aluminum oxide (Al_2O_3) was integrated into the mix. Al_2O_3, known for its combustion-enhancing properties, did increase the combustion efficiency of the fuel. Yet, this came at the cost of a 6.08% escalation in NOx emissions for the HCCI-DI engine utilizing WCO.

Figure 6 presents a comprehensive visual representation of hydrocarbon (HC) emissions resulting from the combustion process in both direct injection (DI) and homogeneous charge compression ignition-direct injection (HCCI-DI) setups. These are further delineated based on the presence or absence of aluminum oxide (Al_2O_3) as an additive. A discernible trend emerges from the experimental data: there is a consistent decline in HC emissions as the engine load intensifies. This decreasing trend might be attributed to more complete combustion at higher loads, which leads to fewer unburnt hydrocarbons. One of the key factors influencing this trend is the inherent oxygen-rich profile of the waste cooking oil (WCO) biodiesel. The elevated oxygen content ensures a more thorough and efficient combustion process, effectively reducing the volume of unburnt hydrocarbons that typically account for HC emissions. In conjunction with this, the inclusion of Al_2O_3 as an additive augments the combustion process even further. Al_2O_3, known for its combustion-enhancing properties, ensures a more complete burn, further mitigating the potential for HC emissions due to incomplete combustion. The comparative analysis between different fuel types offered intriguing insights. For instance, when WCO biodiesel was employed in a DI combustion setting, there was a significant reduction in HC emissions by 33.93% compared to traditional diesel-fueled DI combustion. This underscores the environmental benefits of WCO biodiesel, showcasing its potential as a cleaner alternative fuel source. However, it is crucial to highlight that not all advancements yielded positive outcomes in terms of HC emissions. Despite its benefits in

https://doi.org/10.1021/acsomega.3c05959
ACS Omega 2023, 8, 47701−47713

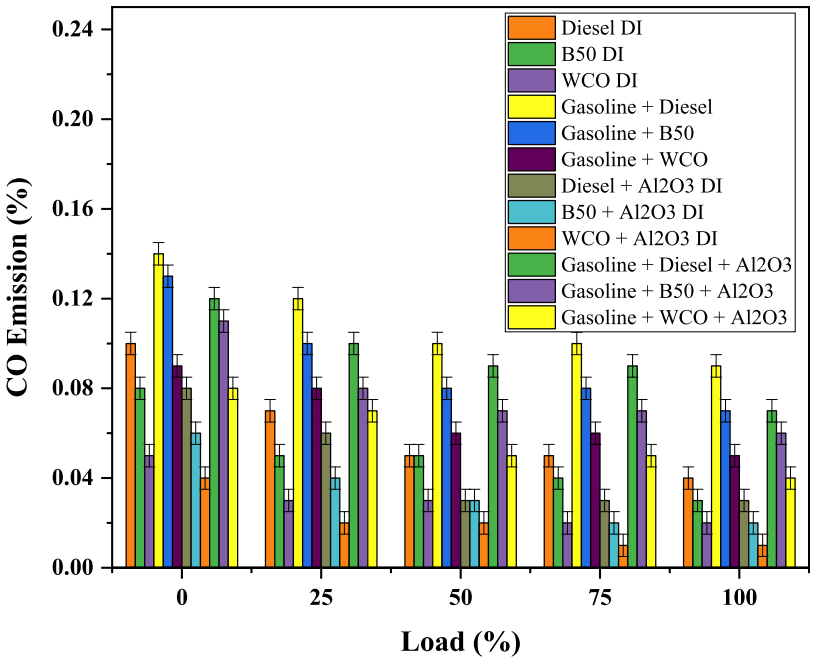

Figure 8. Effects of Al_2O_3 on CO.

other areas, the use of HCCI-DI combustion, especially when petrol was employed as a premix, led to a surge in HC emissions. This is likely due to the lower combustion temperatures and leaner mixtures associated with HCCI-DI. Such conditions can sometimes result in incomplete combustion, leading to a rise in unburnt hydrocarbons.

Figure 7 provides a detailed graphical representation of the relationship between engine load and smoke emissions when utilizing biodiesel. A clear trend can be discerned from the data: as the engine load intensifies, smoke emissions from the biodiesel engine see a proportional increase. This rise in smoke emissions with increased load might be attributable to the higher fuel consumption rate and consequent incomplete combustion under heavier loads, producing more particulate matter, which manifests as visible smoke. Interestingly, the data reveals a positive shift when a certain additive is introduced to the biodiesel. The introduction of fuel to the biodiesel mix led to a significant attenuation of smoke emissions, showing a marked reduction of 39.21%. This indicates that the additive not only enhances the combustion characteristics of biodiesel but also contributes to a cleaner burn with fewer particulate emissions. This could be due to improved fuel atomization, better fuel−air mixing, or enhanced combustion efficiency, resulting in fewer unburnt particles being released. Another noteworthy observation is the influence of aluminum oxide (Al_2O_3) when added to the fuel mix. Al_2O_3, renowned for its combustion-enhancing properties, further optimized the burning process, especially as the biodiesel content in the fuel mix increased. This additive, by promoting a more complete and efficient combustion process, acts as a significant deterrent to smoke emissions. The presence of Al_2O_3 seems to counteract the inherent tendencies of biodiesel to produce smoke, especially at higher concentrations, leading to a cleaner exhaust profile. In essence, while smoke emissions of biodiesel exhibit an increasing trend with the load, strategic interventions in the form of fuel additives and the incorporation of Al_2O_3 can significantly mitigate this challenge, fostering a cleaner and more environmentally friendly combustion process.

Figure 8 offers a clear visualization of the impact of fuel premixing on carbon monoxide (CO) emissions. It can be gleaned from the presented data that the nature of the fuel, its constituents, and the combustion process play significant roles in determining CO emission levels. One of the salient features of biodiesel is its inherently lower carbon content coupled with enhanced oxygen availability. These properties ensure that there is more efficient combustion, which, in turn, leads to decreased CO emissions. CO is typically produced during incomplete combustion; therefore, the more complete the combustion, the fewer the CO emissions that are expected. This assertion is supported by observations from direct injection combustion, where biodiesel facilitated a remarkable reduction in the level of CO emissions by up to 50%.

7. DESIGN OF THE ANN MODEL

The research utilized ANN as a technique to precisely predict output variables. ANNs may learn the link between the variables of input and output by analyzing the data that is currently available, even when complete knowledge about a system is not accessible. The study's five outcome parameters were thermal efficiency, NOx, HC, smoke, and CO, whereas its four input variables were load, fuel mix, PFR, and the Al_2O_3 additive. The mean square error (MSE), which has advantageous qualities for optimization, was employed as the loss function in the study, which utilized a multilayer FFN model with a log-sigmoid function of activation in the hidden and output neurons. The model's accuracy was increased, and using eq 5, all values were normalized to fall between 0 and 1, preventing any one parameter from having an undue impact on the output variables.

$$v^* = \frac{(v - v_{min})}{(v_{max} - v_{min})} \quad (5)$$

https://doi.org/10.1021/acsomega.3c05959
ACS Omega 2023, 8, 47701−47713

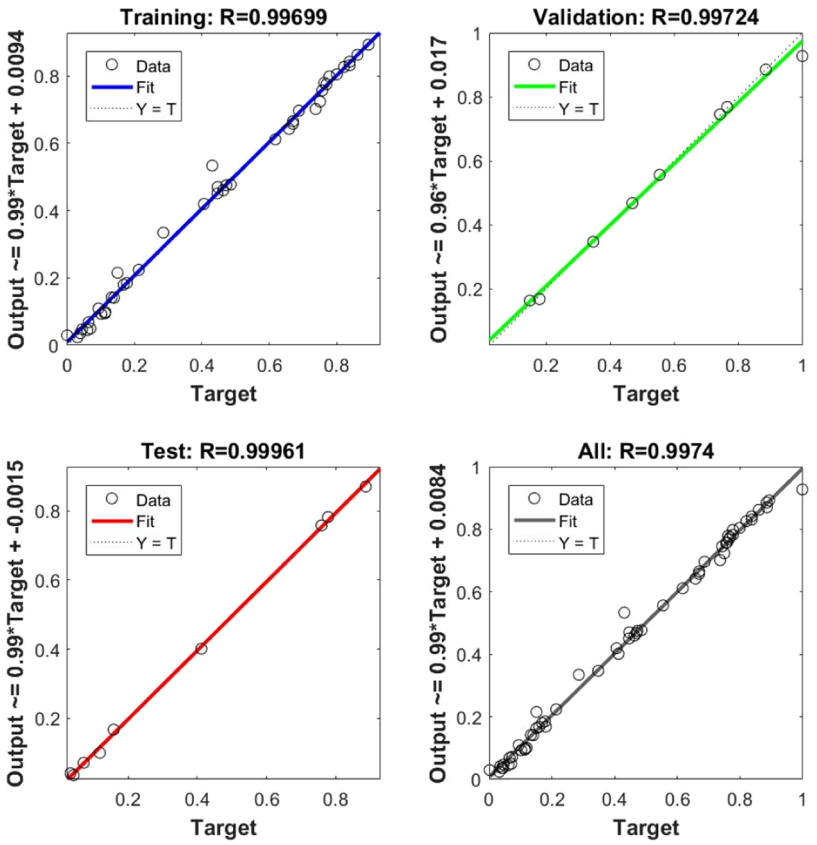

Figure 9. Correlation coefficients of the developed network.

where, v^* represents the normalized value of v. After the equation is applied, v^* will be a value between 0 and 1, inclusive. v is the current value that one wants to normalize. It can be any real number, but for the normalization to make sense, it should ideally fall between v_{min} and v_{max}. v_{min} is the minimum value in the data set or the range of values one is working with. In the context of the equation, it is the value that will be scaled to 0 after normalization. v_{max} is the maximum value in the data set or the range of values one is working with. Similarly, in the context of the equation, it is the value that will be scaled to 1 after normalization.

To preserve the impact of each parameter on the output variables and make the model more precise, all of the variables in this research were converted to a range of 0−1. Using the inverse of eq 5, the normalization procedure was reversed to yield the real values. The NRMSE and MAPE measures of statistical error were utilized by researchers to evaluate the suggested ANN model's accuracy. Equations 6 through 8 define the NRMSE and MAPE, two metrics for measuring prediction error.

$$\text{NRMSE} = \frac{\text{RSME}}{(t_{max} - t_{min})} \tag{6}$$

where

$$\text{RMSE} = \sqrt{\frac{1}{m}\sum_{i=1}^{m}(t_i - o_i)^2} \tag{7}$$

$$\text{MAPE} = \frac{1}{m}\sum_{i=1}^{m}\left(\left|\frac{t_i - o_i}{t_i}\right|\right) \times 100 \tag{8}$$

By measuring the correlation between the suggested ANN model's predicted values and actual values using R and R^2, the recommended ANN model was assessed. These metrics, which are used to determine how accurate the model is, are defined by eqs 9 and 10, respectively.

$$R = \sqrt{1 - \frac{\sum_{i=1}^{m}((t_i - o_i)^2)}{\sum_{i=1}^{m} o_i^2}} \tag{9}$$

$$R^2 = 1 - \frac{\sum_{i=1}^{m}((t_i - o_i)^2)}{\sum_{i=1}^{m} o_i^2} \tag{10}$$

Figure 9 demonstrates how the correlation coefficient (R) was used to assess the suggested ANN model's accuracy. The findings demonstrated that the R values for the training, test, and validation data were extremely close to 1, demonstrating the model's capability to make precise predictions.

As shown in Table 4, the model's performance was further evaluated using the NRMSE, MAPE, R, and R2 values. These statistics show that the ANN model provided extremely

Table 4. Error and Performance Metrics for ANN Predictions

parameter	NRMSE (%)	MAPE (%)	R	R^2
η_{bth}	0.013975	0.002521	0.999835	0.99967
NOx	0.022718	0.010266	0.999227	0.998454
HC	0.032168	0.036367	0.998262	0.996526
smoke	0.028567	0.200946	0.996122	0.992259
CO	0.041425	0.017132	0.997825	0.995655

https://doi.org/10.1021/acsomega.3c05959
ACS Omega 2023, 8, 47701−47713

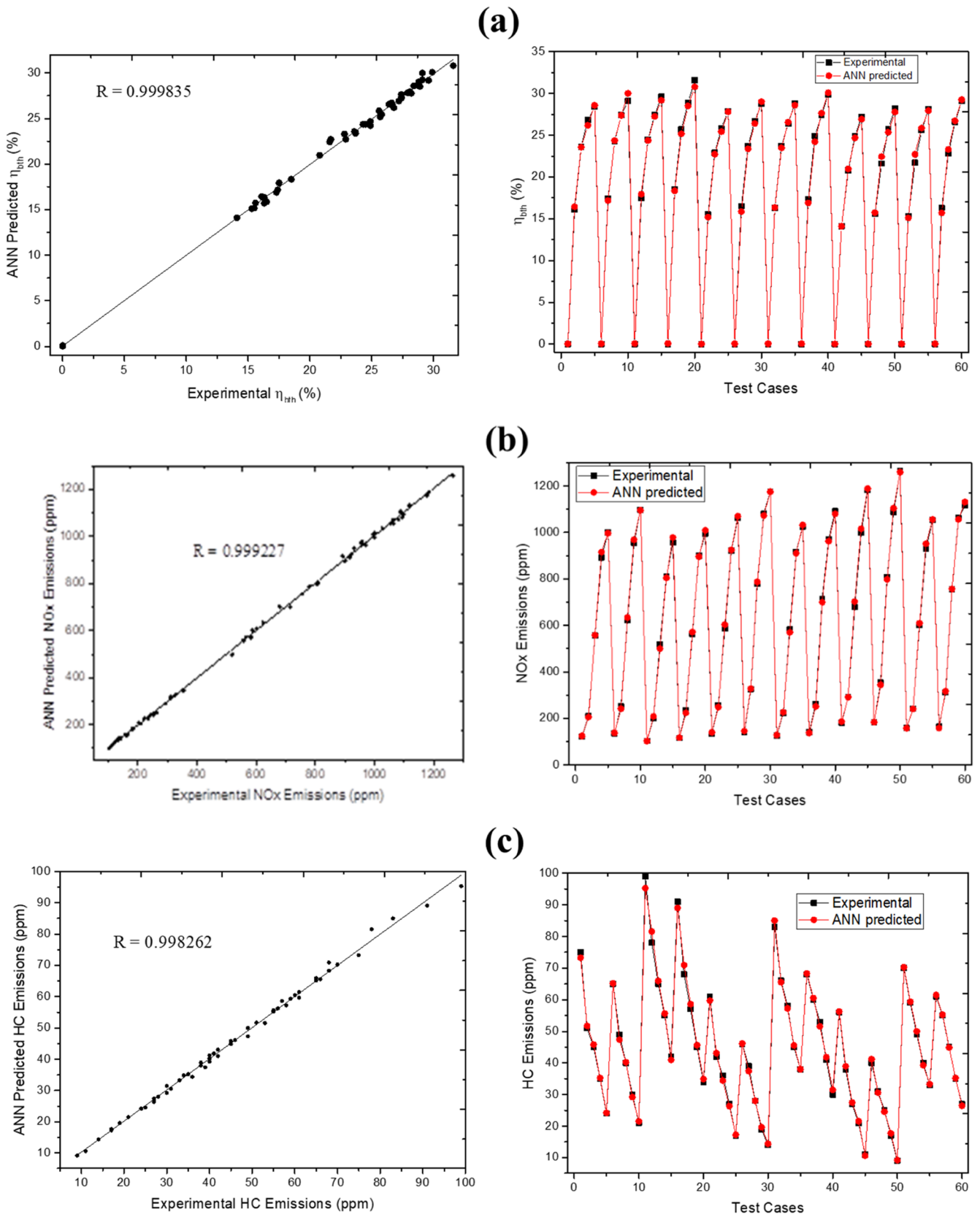

Figure 10. Comparison of experimental data and ANN predictions for (a) η_{bth}, (b) NOx, (c) HC, (d) smoke, and (e) CO.

accurate predictions, with low NRMSE and MAPE values and R and R2 values close to 1.

Figure 10 compares the experimental findings for NOx, HC, smoke, and CO emissions, as well as the BSFC, to the predictions produced by the ANN model. The comparison highlights the ANN model's greater simulation capabilities by demonstrating how well the predictions from the ANN model match the experimental data.

https://doi.org/10.1021/acsomega.3c05959
ACS Omega 2023, 8, 47701−47713

8. REGRESSION MODELING

In order to forecast the output variables of (η_{bth}), NOx, HC, smoke, and CO, regression analysis was performed in this study. As input parameters, load, fuel mixture, PFR, and Al_2O_3 additive were taken into account. The fuel combination contained 0−100% WCO biodiesel, and from 0−100% of the engine's maximum load, the load changed. The PFR values ranged from 0 to 0.2, whereas the Al_2O_3 additive concentrations ranged from 0 to 3 mg/L. The acquired data were utilized to build second-order polynomial models using eq 11.[44]

$$y = \beta_0 + \sum_{i=1}^{4} \beta_i X_i + \sum_{i-1}^{4} \beta_{ii} X_i^2 + \sum_{i<1}^{4} \beta_{ij} X_i X_j + \varepsilon \quad (11)$$

Regression analysis was utilized to project the study's outcomes, including η_{bth}, NOx, HC, smoke, and CO. The Al_2O_3 additive concentration ($C_{Al_2O_3}$), fuel blend (FB), PFR, and load (L) input variables were chosen. With these inputs, second-degree polynomial models were created. These models, which comprised the full linear terms, interaction terms, and quadratic terms of the four inputs, were defined using eqs 12 through 16.

$$\begin{aligned}\eta_{bth} = {} & 0.942 + 0.6343\cdot L - 0.0045\cdot FB + 2.10\cdot PFR \\ & + 0.116\cdot C_{Al_2O_3} - 0.003651\cdot L^2 - 0.000042\cdot FB^2 \\ & - 0.000117\cdot L\cdot FB + 0.0453\cdot L\cdot PFR \\ & + 0.00284\cdot L\cdot C_{Al_2O_3} - 0.0160\cdot FB\cdot PFR \\ & - 0.00027\cdot FB\cdot Al_2O_3 + 0.37\cdot PFR\cdot C_{Al_2O_3}\end{aligned} \quad (12)$$

$$\begin{aligned}NOx = {} & 43.2 + 9.44\cdot L + 1.082\cdot FB + 180\cdot PFR \\ & - 5.0\cdot C_{Al_2O_3} + 0.00307\cdot L^2 - 0.00332\cdot FB^2 \\ & + 0.00894\cdot L\cdot FB - 2.27\cdot L\cdot PFR - 0.230\cdot L\cdot C_{Al_2O_3} \\ & - 2.44\cdot FB\cdot PFR + 0.010\cdot FB\cdot C_{Al_2O_3} \\ & - 67.6\cdot PFR\cdot C_{Al_2O_3}\end{aligned} \quad (13)$$

$$\begin{aligned}HC = {} & 72.44 - 0.5973\cdot L - 0.3275\cdot FB + 111.50\cdot PFR \\ & - 3.000\cdot C_{Al_2O_3} + 0.001105\cdot L^2 + 0.000940\cdot FB^2 \\ & + 0.001390\cdot L\cdot FB - 0.180\cdot L\cdot PFR \\ & + 0.01556\cdot L\cdot C_{Al_2O_3} - 0.0100\cdot FB\cdot PFR \\ & + 0.00400\cdot FB\cdot C_{Al_2O_3} - 1.22\cdot PFR\cdot C_{Al_2O_3}\end{aligned} \quad (14)$$

$$\begin{aligned}smoke = {} & 0.179 - 0.02710\cdot L - 0.00090\cdot FB + 0.28\cdot PFR \\ & - 0.0157\cdot C_{Al_2O_3} + 0.000611\cdot L^2 + 0.000005\cdot FB^2 \\ & - 0.000028\cdot L\cdot FB - 0.0431\cdot L\cdot PFR \\ & - 0.001031\cdot L\cdot C_{Al_2O_3} + 0.0055\cdot FB\cdot PFR \\ & + 0.000310\cdot FB\cdot C_{Al_2O_3} + 0.194\cdot PFR\cdot Al_2O_3\end{aligned} \quad (15)$$

$$\begin{aligned}CO = {} & 0.09775 - 0.001272\cdot L - 0.000395\cdot FB \\ & + 0.2400\cdot PFR - 0.00333\cdot C_{Al_2O_3} + 0.000008\cdot L^2 \\ & - 0.000000\cdot FB^2 + 0.000002\cdot L\cdot FB \\ & - 0.000267\cdot L\cdot PFR + 0.000027\cdot L\cdot C_{Al_2O_3} \\ & - 0.000400\cdot FB\cdot PFR - 0.000000\cdot FB\cdot C_{Al_2O_3} \\ & - 0.01222\cdot PFR\cdot C_{Al_2O_3}\end{aligned} \quad (16)$$

By calculating the NRMSE, MAPE, R, and R^2 using the formulas 5−9, the correctness of the regression model was evaluated. The results of Table 4 show that the predictions of the model were highly accurate and had a small range of error values. For CO emissions, the largest NRMSE was 0.12%, while for smoke emissions, the greatest MAPE was 1.33%. The R and R2 values were found to be close to 1, demonstrating a strong correlation between the predicted and observed values.

9. COMPARISON OF ANN AND REGRESSION MODEL PREDICTIONS WITH EXPERIMENTAL RESULTS

The outputs of the proposed ANN and regression models closely matched each other when compared to the experimental data, demonstrating the high accuracy of both models. Table 5 displays the results for η_{bth}, HC, smoke, CO, and NOx from the experimental data as well as from the ANN and regression models for three sets of input variables that were randomly selected. Table 6 shows how well-replicated the output variables may be using both regression and ANN models.

Table 5. Error and Performance Metrics for Regression Model Predictions

parameter	NRMSE (%)	MAPE (%)	R	R^2
η_{bth}	0.044997	0.03672	0.998282	0.996566
NOx	0.057482	0.194903	0.99499	0.990006
HC	0.028611	0.000311	0.998663	0.997328
smoke	0.074047	1.332608	0.972026	0.944835
CO	0.10763	0.057269	0.987043	0.974254

The experimental results and those predicted by the regression and ANN models may be compared, showing how accurate both models' simulations are given that the projected values are quite close to the real data.

10. CONCLUSIONS

Experimental research was conducted on gasoline premixed waste cooking oil (WCO), which was used as the direct injection fuel, and aluminum oxide (Al_2O_3), which was used as the fuel additive, in an HCCI-DI engine. The results obtained were then compared to those from diesel-fueled DI combustion. Both an artificial neural network (ANN) and a regression modeling approach were used to predict the values of η_{bth}, HC, smoke, and CO, as well as NOx. The study found the following.

1. The study underscores the profound impact of fuel types and additives on combustion characteristics. Utilizing WCO biodiesel in engines leads to an increment in the start of combustion (SOC) and a decrement in peak pressure (P_{max}) values due to its higher viscosity and lower calorific value. The addition of Al_2O_3 enhances the

https://doi.org/10.1021/acsomega.3c05959
ACS Omega 2023, 8, 47701−47713

Table 6. Comparison of ANN and Regression Model Predictions with Experimental Results

L (%)	FB (%)	PFR	$C_{Al_2O_3}$ (mg/L)	responses		experimental	ANN	regression model
100	0	0.2	0	η_{bth}	%	29.6	29.605	29.188
				NOx	ppm	959	960.545	960.5
				HC	ppm	42	42.072	42.46
				smoke	FSN	2.76	2.756	2.773
				CO	%	0.09	0.091	0.09321
50	100	0	3	η_{bth}	%	24.3	24.577	24.7675
				NOx	ppm	806	805.437	806.075
				HC	ppm	25	25.033	25.4715
				smoke	FSN	0.17	0.170	0.172
				CO	%	0.02	0.021	0.023
100	50	0.2	3	η_{bth}	%	29.9	30.022	29.495
				NOx	ppm	1092	1091.795	1092.54
				HC	ppm	30	30.176	30.821
				smoke	FSN	2.63	2.835	2.862
				CO	%	0.06	0.061	0.06

P_{max} values, making it an effective additive to improve the combustion efficiency of biodiesels.

2. Al_2O_3, when added to fuels, has shown promising enhancements in braking thermal efficiency (η_{bth}) of the engines, especially when used with WCO biodiesel. The thermal efficiency (η_{bth}) of the HCCI-DI engine that ran on WCO biodiesel fuel increased by up to 4.23%. As a fuel additive, Al_2O_3 was added to the petrol, which increased η_{bth} by up to an additional 6.76%.
3. NOx emissions tend to increase with load and with the use of WCO biodiesel, primarily due to higher cylinder temperatures. However, the HCCI-DI mechanism with gasoline premixing mitigates these emissions, reflecting the benefits of adopting alternative combustion strategies.
4. Both WCO biodiesel and Al_2O_3 have demonstrated a capacity to significantly reduce HC and smoke emissions, thus rendering the combination an environmentally favorable choice for combustion engines. Utilizing Al_2O_3 gasoline additive reduced smoke emissions by up to 25.99%.
5. Both ANN and regression models provided accurate predictions when validated against experimental data. The correlation coefficients (R) were very close to 1, indicating strong accuracy. These predictive models can be immensely useful for foreseeing engine behavior under different conditions and fuel mixtures.

AUTHOR INFORMATION

Corresponding Author

Subramanian Manivel − *Department of Mechanical Engineering, St. Joseph's College of Engineering, Chennai 600119 Tamil Nadu, India;* orcid.org/0000-0002-8117-9529; Email: subramanianm@stjosephs.ac.in

Authors

Lionus Leo George Mary − *Department of Mechanical Engineering, St. Joseph's College of Engineering, Chennai 600119 Tamil Nadu, India*

Shalini Garg − *MIT Art Design and Technology University, Pune 412201 Maharashtra, India*

Vinoth Babu Nagam − *Department of Mechanical Engineering, Rajalakshmi Engineering College, Chennai 602105 Tamil Nadu, India*

Komal Garse − *Department of Mechanical Engineering, Sinhgad College of Engineering, Pune 411041 Maharashtra, India*

Ranjit Mali − *Department of Mechanical Engineering, Sinhgad College of Engineering, Pune 411041 Maharashtra, India*

T. M. Yunus Khan − *Department of Mechanical Engineering, College of Engineering, King Khalid University, Abha 61421, Saudi Arabia;* orcid.org/0000-0002-9242-7591

Rahmath Ulla Baig − *Department of Industrial Engineering, College of Engineering, King Khalid University, Abha 61421, Saudi Arabia*

Complete contact information is available at: https://pubs.acs.org/10.1021/acsomega.3c05959

Notes

The authors declare no competing financial interest.

ACKNOWLEDGMENTS

The authors extend their appreciation to the Deanship of Scientific Research at King Khalid University for funding this work through research groups program under grant number R.G.P 2/118/44.

REFERENCES

(1) Qian, Y.; Li, H.; Han, D.; Ji, L.; Huang, Z.; Lu, X. Octane rating effects of direct injection fuels on dual fuel HCCI-DI stratified combustion mode with port injection of n-heptane. *Energy* **2016**, *111*, 1003−1016.

(2) Onishi, S.; Jo, S. H.; Shoda, K.; Jo, P. D.; Kato, S. Active thermo-atmosphere combustion (ATAC)—a new combustion process for internal combustion engines. *SAE Trans.* **1979**, 1851−1860.

(3) Noguchi, M.; Tanaka, Y.; Tanaka, T.; Takeuchi, Y. A study on gasoline engine combustion by observation of intermediate reactive products during combustion. *SAE Trans.* **1979**, 2816−2828.

(4) Najt, P. M.; Foster, D. E. Compression-ignited homogeneous charge combustion. *SAE Trans.* **1983**, 964−979.

(5) Iida, N. Combustion analysis of methanol-fueled active thermo-atmosphere combustion (ATAC) engine using a spectroscopic observation. *SAE Trans.* **1994**, 1169−1184.

(6) Christensen, M.; Hultqvist, A.; Johansson, B. Demonstrating the multi fuel capability of a homogeneous charge compression ignition engine with variable compression ratio. *SAE Trans.* **1999**, 2099−2113.

(7) Wåhlin, F.; Cronhjort, A. *Fuel sprays for premixed compression ignited combustion-characteristics of impinging sprays (No. 2004−01−1776). SAE Technical Paper*, 2004.

(8) Boyarski, N. J.; Reitz, R. D. Premixed compression ignition (PCI) combustion with modeling-generated piston bowl geometry in a diesel engine. *SAE Trans.* **2006**, 133−143.
(9) Christensen, M.; Johansson, B.; Amnéus, P.; Mauss, F. Supercharged homogeneous charge compression ignition. *SAE Trans.* **1998**, 1129−1144.
(10) Iwabuchi, Y.; Kawai, K.; Shoji, T.; Takeda, Y. *Trial of new concept diesel combustion system-premixed compression-ignited combustion (No. 1999−01−0185). SAE Technical Paper*, 1999.
(11) Kanda, T.; Hakozaki, T.; Uchimoto, T.; Hatano, J.; Kitayama, N.; Sono, H. PCCI operation with early injection of conventional diesel fuel. *SAE Trans.* **2005**, 584−593.
(12) Petitdidier, A. *Practical investigation of noise reduction of a diesel passenger car (No. 790447). SAE Technical Paper*, 1979.
(13) Wimmer, A.; Eichlseder, H.; Klell, M.; Figer, G. Potential of HCCI concepts for DI diesel engines. *Int. J. Veh. Des.* **2006**, *41* (1−4), 32−48.
(14) Zheng, J.; Caton, J. A. Effects of operating parameters on nitrogen oxides emissions for a natural gas fueled homogeneous charged compression ignition engine (HCCI): Results from a thermodynamic model with detailed chemistry. *Appl. Energy* **2012**, *92*, 386−394.
(15) Nishi, M.; Kanehara, M.; Iida, N. Assessment for innovative combustion on HCCI engine by controlling EGR ratio and engine speed. *Appl. Therm. Eng.* **2016**, *99*, 42−60.
(16) Ikemoto, M.; Kojima, Y.; Iida, N. *Development of the control system using EGR for the HCCI engine running on DME (No. 2005−32−0062). SAE Technical Paper*, 2005.
(17) Kanoto, Y.; Ohmura, T.; Iida, N. *An investigation of combustion control using EGR for small and light HCCI engine fuelled with DME (No. 2007−01−1876). SAE Technical Paper*, 2007.
(18) Jung, D.; Iida, N. Closed-loop control of HCCI combustion for DME using external EGR and rebreathed EGR to reduce pressure-rise rate with combustion-phasing retard. *Appl. Energy* **2015**, *138*, 315−330.
(19) Krishnan, S. R.; Srinivasan, K. K.; Raihan, M. S. The effect of injection parameters and boost pressure on diesel-propane dual fuel low temperature combustion in a single-cylinder research engine. *Fuel* **2016**, *184*, 490−502.
(20) Hyvönen, J.; Haraldsson, G.; Johansson, B. Supercharging HCCI to extend the operating range in a multi-cylinder VCR-HCCI engine. *SAE Trans.* **2003**, 2456−2468.
(21) Tanaka, S.; Ayala, F.; Keck, J. C.; Heywood, J. B. Two-stage ignition in HCCI combustion and HCCI control by fuels and additives. *Combust. Flame* **2003**, *132* (1−2), 219−239.
(22) Ying, W.; Li, H.; Jie, Z.; Longbao, Z. Study of HCCI-DI combustion and emissions in a DME engine. *Fuel* **2009**, *88* (11), 2255−2261.
(23) Das, P.; Selokar, M.; Subbarao, P. M. V.; Subrahmanyam, J. P. *Effect of injection timing, premixed equivalence ratio and EGR on combustion characteristics of an HCCI-DI combustion engine using in-cylinder dual injection strategy (No. 2016−01−0752). SAE Technical Paper*, 2016.
(24) Wan Ghazali, W. N. M.; Mamat, R.; Masjuki, H. H.; Najafi, G. Effects of biodiesel from different feedstocks on engine performance and emissions: A review. *Renewable Sustainable Energy Rev.* **2015**, *51*, 585−602.
(25) Hadavi, S. A.; Li, H.; Przybyla, G.; Jarrett, R.; Andrews, G. Comparison of gaseous emissions for B100 and diesel fuels for real world urban and extra urban driving. *SAE Int. J. Fuels Lubr.* **2012**, *5* (3), 1132−1154.
(26) Hwang, J.; Bae, C.; Gupta, T. Application of waste cooking oil (WCO) biodiesel in a compression ignition engine. *Fuel* **2016**, *176*, 20−31.
(27) Sadhik Basha, J.; Anand, R. B. Role of nanoadditive blended biodiesel emulsion fuel on the working characteristics of a diesel engine. *J. Renewable Sustainable Energy* **2011**, *3* (2), No. 023106, DOI: 10.1063/1.3575169.
(28) Attia, A. M.; El-Seesy, A. I.; El-Batsh, H. M.; Shehata, M. S. In *Effects of Alumina Nanoparticles Additives into Jojoba Methyl Ester-diesel Mixture on Diesel Engine Performance*, ASME International Mechanical Engineering Congress and Exposition (Vol. 46521, p. V06BT07A019); American Society of Mechanical Engineers, 2014.
(29) Sadhik Basha, J.; Anand, R. B. The influence of nano additive blended biodiesel fuels on the working characteristics of a diesel engine. *J. Braz. Soc. Mech. Sci. Eng.* **2013**, *35*, 257−264.
(30) Venkatesan, S. P.; Kadiresh, P. N. Influence of an aqueous cerium oxide nanofluid fuel additive on performance and emission characteristics of a compression ignition engine. *Int. J. Ambient Energy* **2016**, *37* (1), 64−67.
(31) Arul Mozhi Selvan, V.; Anand, R. B.; Udayakumar, M. Effect of Cerium Oxide Nanoparticles and Carbon Nanotubes as fuel-borne additives in Diesterol blends on the performance, combustion and emission characteristics of a variable compression ratio engine. *Fuel* **2014**, *130*, 160−167.
(32) Keskin, A.; Gürü, M.; Altıparmak, D. Influence of tall oil biodiesel with Mg and Mo based fuel additives on diesel engine performance and emission. *Bioresour. Technol.* **2008**, *99* (14), 6434−6438.
(33) Venu, H.; Madhavan, V. Effect of Al_2O_3 nanoparticles in biodiesel-diesel-ethanol blends at various injection strategies: Performance, combustion and emission characteristics. *Fuel* **2016**, *186*, 176−189.
(34) Tinaut, F. V.; Melgar, A.; Gimenez, B.; Reyes, M. Prediction of performance and emissions of an engine fuelled with natural gas/hydrogen blends. *Int. J. Hydrogen Energy* **2011**, *36* (1), 947−956.
(35) Yusaf, T. F.; Yousif, B. F.; Elawad, M. M. Crude palm oil fuel for diesel-engines: Experimental and ANN simulation approaches. *Energy* **2011**, *36* (8), 4871−4878.
(36) Sharon, H.; Jayaprakash, R.; Sundaresan, A.; Karuppasamy, K.; et al. Biodiesel production and prediction of engine performance using SIMULINK model of trained neural network. *Fuel* **2012**, *99*, 197−203.
(37) Yap, W. K.; Ho, T.; Karri, V. Exhaust emissions control and engine parameters optimization using artificial neural network virtual sensors for a hydrogen-powered vehicle. *Int. J. Hydrogen Energy* **2012**, *37* (10), 8704−8715.
(38) Gurunathan, B.; Ravi, A. Biodiesel production from waste cooking oil using copper doped zinc oxide nanocomposite as heterogeneous catalyst. *Bioresour. Technol.* **2015**, *188*, 124−127.
(39) Dasari, S. R.; Goud, V. V. Effect of pre-treatment on solvents extraction and physico-chemical properties of castor seed oil. *Journal of Renewable and Sustainable Energy* **2014**, *6* (6), No. 063108.
(40) Senthur Prabu, S.; Asokan, M. A.; Roy, R.; Francis, S.; Sreelekh, M. K. Performance, combustion and emission characteristics of diesel engine fuelled with waste cooking oil bio-diesel/diesel blends with additives. *Energy* **2017**, *122*, 638−648.
(41) Gattamaneni, R. N. L.; Subramani, S.; Santhanam, S.; Kuderu, R. Combustion and emission characteristics of diesel engine fuelled with rice bran oil methyl ester and its diesel blends. *Therm. Sci.* **2008**, *12* (1), 139−150.
(42) Hwang, J.; Qi, D.; Jung, Y.; Bae, C. Effect of injection parameters on the combustion and emission characteristics in a common-rail direct injection diesel engine fueled with waste cooking oil biodiesel. *Renewable Energy* **2014**, *63*, 9−17.
(43) Sadeghinezhad, E.; Kazi, S. N.; Sadeghinejad, F.; Badarudin, A.; Mehrali, M.; Sadri, R.; Safaei, M. R. A comprehensive literature review of bio-fuel performance in internal combustion engine and relevant costs involvement. *Renewable Sustainable Energy Rev.* **2014**, *30*, 29−44.
(44) Benardos, P. G.; Vosniakos, G. C. Predicting surface roughness in machining: a review. *Int. J. Mach. Tools Manuf.* **2003**, *43* (8), 833−844.

https://doi.org/10.1021/acsomega.3c05959
ACS Omega 2023, 8, 47701−47713